CrossMark

Solar light-assisted photocatalytic degradation of methylene blue with Mo/TiO$_2$: a comparison with Cr- and Ni-doped TiO$_2$

Sushil M. Chaudhari[1] · Pramod M. Gawal[1] · Priyanka K. Sane[1] · Sharad M. Sontakke[1] · Parag R. Nemade[1,2]

Abstract Highly active Cr-doped, Ni-doped and Mo-doped TiO$_2$ photocatalysts were synthesized by a sol–gel method. The synthesized catalysts were characterized by UV–DRS, BET, XRD, FE-SEM–EDS, TEM and XPS. Metal doping decreased the band gap of TiO$_2$ to 2.83 eV for Mo-doped TiO$_2$ and Ni-doped TiO$_2$. The activity of the synthesized photocatalysts was evaluated by studying the degradation of MB as a model pollutant under both UV and solar irradiation. The Mo/TiO$_2$ catalyst achieved 98% degradation under solar light within 120 min. The activity of the catalysts was in the order Ni-doped TiO$_2$ < Cr-doped TiO$_2$ < TiO$_2$ < Mo-doped TiO$_2$. The optimum activity was found at a loading of 1.5 g/L of Mo-doped TiO$_2$ under both UV and solar irradiation. The degradation was rapid at pH > 7 and followed pseudo-first order kinetics. Degradation by-products were analyzed on HR-LCMS and a mechanism is proposed.

Keywords Mo-doped TiO$_2$ · Cr-doped TiO$_2$ · Ni-doped TiO$_2$ · Dye degradation · MB · UV light · Visible light

✉ Parag R. Nemade
pr.nemade@ictmumbai.edu.in

1   Department of Chemical Engineering, Institute of Chemical Technology, Mumbai, India

2   Department of Oils, Oleochemicals and Surfactant Technology, Institute of Chemical Technology, Mumbai, India

Introduction

Contamination of water with hazardous chemicals is a serious concern for the environment as well as for human health. Many of these chemical contaminants are non-biodegradable, highly toxic, possess complex chemical structures and are recalcitrant to conventional water treatment processes. Dyes are one such class of pollutants found commonly in the effluents of plastic, paper, textile, cosmetics and several other chemical industries [1]. The textile industry generates large amounts of dye-containing effluents during processing [2]. The release of such polluted water into the ecosystem causes soil contamination and becomes a threat to aquatic life [3]. Therefore, treatment of these effluents before its release into the environment is very important. Several physical, chemical and biological processes, which include coagulation, adsorption, filtration, hydrogen peroxide addition, reverse osmosis, electrochemical oxidation, biodegradation, ozonation, etc., are reported to remove dye pollutants [2–10]. However, most of these methods suffer from certain limitations. For example, coagulation transforms the pollutants from one phase to another rather than removing them. Chlorination results in the formation of complex compounds like haloacetic acid and trihalomethane, which are potentially carcinogenic. Adsorption concentrates dye solutions that need to be subsequently treated. Dyes foul reverse osmosis/nanofiltration membranes limiting membrane life. Most dyes do not undergo biological degradation and remain undegraded. Advanced oxidation processes such as the use of hydrogen peroxide, ozonation or electrochemical oxidation can potentially mineralize dyes, but are expensive. Ozone is a respiratory irritant and ground-level ozone pollution from unreacted ozonolysis is a major health hazard [11].

Among advanced oxidation processes, photocatalysis is receiving increasing attention due to its distinct advantages over conventional water treatment processes. Semiconductor photocatalysis using TiO_2 has shown a great potential to remove a wide range of chemical and microbial pollutants. TiO_2 only absorbs in the UV region (band gap: 3.2 eV). For a green process, minimum energy needs to be expended, and therefore solar light becomes the primary photo-energy source. In solar radiation, only about 5% of the total energy is in the UV region, while the majority of solar insolation is in the visible wavelengths. A catalyst can be made to absorb visible light by decreasing its band gap. Therefore, the scientific community has focused their attention towards visible light photocatalysis [12–15]. Visible light absorption of TiO_2 has been enhanced by doping the TiO_2. Several transition metal ions have been investigated as dopants in earlier reports [16–21]. It is observed that the photocatalytic properties of TiO_2 are governed by different locations of the dopants in the host matrix [22].

Doping TiO_2 with Fe^{3+}, Mo^{5+}, Ru^{3+}, Os^{3+}, Re^{5+}, Cr^{3+}, Ni^{2+}, etc. at concentrations of 0.1–0.5 wt% significantly increased the photocatalytic activity [23]. Mo^{5+} doping results in a more compact surface with larger surface fluctuations, charge carrier recombination rates and interfacial electron transfer rates, which are beneficial for the absorption of dye molecules [24]. Mo-doped TiO_2 enhances the photocatalytic activity by increasing the surface acidity as well the

oxygen vacancies [25–27]. Doping TiO_2 with Cr narrows the band gap resulting in absorption of light in the visible part of the spectrum, which enhances the photocatalytic degradation of MB dye [20, 28]. Cr-doping increases the temperature of transition of anatase phase TiO_2 to rutile phase [29]. Among the various transition metals, Ni^{2+} appears to be a more efficient dopant for TiO_2. Doping with Ni promotes the lowering of the band gap, enhancing visible light absorption [16]. Ni/TiO_2 exhibits several advantages with respect to uniform particle size, well-defined morphology, crystal structure, and particle size for photocatalysis [30].

The present study aimed to synthesize Cr^{3+}-, Mo^{5+}- and Ni^{2+}-doped TiO_2 catalysts with a lower band gap to shift the absorption edge towards the visible region and enhance the photocatalytic potential of TiO_2. The synthesized catalysts were characterized for crystallinity, band gap, surface area, morphology, elemental composition, and particle size. The activity of the doped catalysts was studied for photocatalytic degradation using methylene blue (MB) as a model substrate under both UV and sunlight. The effect of the type of dopant, catalyst concentration, pH and temperature on the photocatalytic rate was investigated. The degradation byproducts were analyzed using high-resolution liquid chromatography–mass spectroscopy (HR-LCMS), and a possible mechanism of degradation was deduced. The degradation kinetics was studied using the first-order rate law. The novelty of this work is that the catalyst synthesized with only 0.9 wt% Mo/TiO_2 is extremely active, giving complete degradation of MB dye under UV and solar light within 60 and 120 min, respectively.

Materials and methods

Materials

Titanium precursor (titanium (IV) *n*-butoxide, 99% pure) was procured from Alfa Aesar (UK). Molybdenum (V) chloride (95% pure) was obtained from Sigma Aldrich (USA). Nickel (II) nitrate hexahydrate (extrapure), chromium (III) nitrate nonahydrate (98% pure, HPLC grade), ethanol (99.9% pure, AR grade), and nitric acid (69–72%) were purchased from S.D. Fine-Chem, Mumbai, India. MB (98% pure) was procured from Bombay Chemicals, India. Deionized (DI) water was obtained locally from the Millipore Milli-Q system.

Catalyst synthesis

Sol–gel synthesis of TiO_2, Cr/TiO_2, Mo/TiO_2, and Ni/TiO_2 was carried out using a stoichiometric amount of the precursor of titanium and corresponding metals [20, 21, 31, 32].

Titanium *n*-butoxide dissolved in absolute ethanol and distilled water was added to the solution (Ti:H_2O = 1:4 mol basis). The solution was vigorously stirred for 30 min in order to form a sol. After ageing for 24 h, the sol transformed into a gel, which was dried at 120 °C for 2 h and then sintered at 450 °C for 2 h to give TiO_2.

An amount of 62.4 mg of chromium nitrate nonahydrate dissolved in 20 ml of ethanol was added dropwise to a solution of titanium *n*-butoxide in ethanol (20% v/v). The solution thus obtained was stirred for 2 h and aged at room temperature for 12 h to give a gel, which was dried at 80 °C for 12 h and then calcined in a furnace at 500 °C in air for 3 h giving Cr-doped TiO_2.

An amount of 10.5 mg of $MoCl_5$ was dissolved in a solution of 1.5 ml deionized water, 10 ml absolute ethanol and 0.1 ml 70% nitric acid. This solution was added dropwise to a mixture containing 5 ml titanium *n*-butoxide and 20 ml absolute ethanol. The solution thus obtained was stirred for 2–3 h and aged at room temperature for 9–10 h to give a gel, which was dried at 70 °C and then calcined in a furnace at 500 °C in air for 2 h giving Mo-doped TiO_2.

An amount of 5.18 mg of $Ni(NO_3)_3 \cdot 6H_2O$ was dissolved in 3.6 ml deionized water, 5 ml absolute ethanol and 1 ml 70% nitric acid. This solution was added dropwise to a mixture containing 17 ml titanium *n*-butoxide and 40 ml absolute ethanol. The solution thus obtained was stirred for 2–3 h and aged at room temperature for 9–10 h to give a gel, which was dried at 80 °C and then calcined in a furnace at 500 °C in air for 3 h giving Ni-doped TiO_2.

Catalyst characterization

The synthesized catalysts were characterized for their crystal structure by a powder X-Ray diffractometer (Bruker D8 Advance, USA) with a Cu K_α source at a scan rate of $0.1° s^{-1}$. The crystal planes were assigning by comparison with the standard JCPDS database. The crystallite size was calculated from the peak broadening at full width half maximum (FWHM) intensity using the Debye–Scherrer equation. UV–visible diffuse reflectance spectroscopy (Perkin Elmer Lambda-950UV-visible-near infrared spectrometer, USA) was used to estimate the band gap of the synthesized catalysts. Surface area and pore size analysis of the catalyst was estimated from nitrogen adsorption–desorption isotherms using BET apparatus (Micromeritics ASAP-2020 instrument, USA). Inductively coupled plasma–atomic emission spectrometry (ARCOS, Simultaneous ICP Spectromete;, SPECTRO Analytical Instruments, Germany) was used to confirm the amount of dopant. Scanning electron microscope (SEM; JEOL, JSM-7600F, Japan) was also used to identify the morphology of MO/TiO_2 and its elemental composition. High-resolution transmission electron microscopy (PHILIPS CM200, Japan) of MO/TiO_2 was used to image the crystallite features of the catalyst. X-ray photoelectron spectroscopy was conducted in ESCA lab IITB, using an AXIS Supra (Kratos Analytical, UK).

Photocatalytic degradation studies

UV light-assisted photocatalytic degradation experiments were carried out in a batch photocatalytic reactor. A high-pressure mercury vapor lamp (125 W; Philips, India), emitting predominantly at 365 nm (UV-A) was used as a photon source. An open borosilicate glass beaker of 250 ml capacity placed on a magnetic stirrer for

homogeneous mixing was used as the reactor. A detailed description of the reactor setup is described elsewhere [33].

Solar light-assisted photocatalytic degradation experiments were carried out in an open atmosphere where direct sunlight was available. The visible light photocatalytic degradation was performed between 1100 and 1400 hours (Indian Standard Time +5:30 h UTC). The maximum solar light intensity was measured using a Luxmeter (Cetpar, India) and found to be 970 W/m^2.

An amount of 100 ml of a dye solution of the desired concentration was obtained by diluting 1000 ppm stock solution which was charged in the reactor. A specific amount of catalyst was charged and the suspension was stirred for 20 min in the dark to attain adsorption equilibrium and subjected to UV or solar irradiation. Samples were collected every 10 min for analysis. The samples were centrifuged to isolate the catalyst, and the concentration of the solution was then obtained from the absorbance at $\lambda_{max} = 665$ nm. All experiments were repeated at least three times and the mean value is reported along with the standard deviation. The % dye degraded was estimated using Eq. 1, where, C_0 is the initial concentration of dye and C is the concentration of the dye after irradiation time, t.

$$\% \text{ dye degraded} = \frac{C_0 - C}{C_0} \times 100 \tag{1}$$

Degradation byproducts were analyzed using LCMS (G6550A HiP sampler with Dual AJS ESI MS IT PDA detectors; Varian, USA) equipped with a Zorbax Eclipse XDB-C18 column (narrow-bore 2.1 × 150 mm, pore size 5 μm), with a mixture of methanol and water (30:70 v/v) as mobile phase.

Results and discussion

Catalysts characterization

XRD spectra of the sol–gel-synthesized TiO_2, Mo/TiO_2, Cr/TiO_2, and Ni/TiO_2 are shown in Fig. 1. Prominent peaks of anatase phase can be observed for each catalyst and were indexed with reference to the standard powder diffraction pattern (JCPDS 21-1272). The intensities and positions of the peaks were in perfect agreement with the literature values [18, 34]. In addition to anatase, a few low-intensity peaks of the rutile phase were also observed at 27.4° and 42.2°, attributed to the (110) and (200) rutile diffraction planes, respectively, in the spectra of Mo/TiO_2 and Ni/TiO_2 (JCPDS 21-1276). XRD spectra of TiO_2 and Cr/TiO_2 only showed prominent peaks of the anatase phase. The amounts of anatase and rutile phases in the catalysts were estimated from the peak intensities of the XRD spectra of TiO_2, Mo/TiO_2, Cr/TiO_2, and Ni/TiO_2. Mo-doped TiO_2 contained 71.4% anatase and 28.57% rutile, while, in Ni-doped TiO_2, 75.2% anatase and 24.72% rutile phase was observed, and 100% anatase phase was observed in TiO_2 and Cr/TiO_2. The phase transition temperature of anatase to rutile in TiO_2 is approximately 600 °C [35]. The presence of Cr in the TiO_2 matrix increases the anatase–rutile transition temperature to above 600 °C
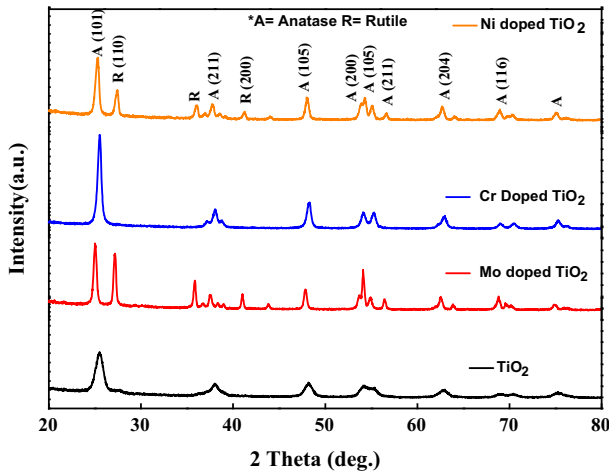
Fig. 1 XRD spectra of TiO_2, Cr/TiO_2, Mo/TiO_2 and Ni/TiO_2 catalysts

[29], while the TiO_2 and Cr/TiO_2 catalysts were calcined to only 500 °C; hence, the rutile phase was not observed. The characteristic peaks of chromium, molybdenum and nickel were not observed in either of the diffraction patterns, which strongly indicated that the dopant ions were substituted in the TiO_2 matrix [18, 20, 31]. The crystallite sizes of the synthesized catalysts were calculated using the Debye–Scherrer equation, and are presented in Table 1. Cr/TiO_2 possessed the smallest crystallite size (23.5 nm) followed by Mo/TiO_2 (28.2 nm) and Ni/TiO_2 (33.4 nm).

The kinetics of the anatase to rutile transition are also affected by metal dopants, which can retard or intensify the phase transition from anatase to rutile [35]. Anatase to rutile transitions are affected in different ways based on the nature of the dopants and the way the dopants have been incorporated in the TiO_2 lattice. In a substitutional solid solution, the dopants substitute atoms in the anatase lattice influencing oxygen vacancies, thereby promoting or inhibiting the transformation to rutile. In an interstitial solid solution, lattice constraints result in stabilization or destabilization, depending on the size, valence, and content effects, again promoting or inhibiting the transformation. In the case of a solid solution, if the solubility limit

Table 1 Material properties of the synthesized catalysts

Catalyst	Crystallite size (nm)	Band gap (eV)	BET (m^2/g)	Pore volume (cm^3/g)	Avg. pore diameter (Å)
Cr/TiO_2	23.5	3.11	23.0	0.041	72
Mo/TiO_2	28.2	2.73	62.1	0.112	72
Ni/TiO_2	33.4	2.71	35.5	0.053	60
TiO_2	13.2	3.23	71.4	0.243	136

of the dopant is exceeded, its precipitation may occur, facilitating phase transformation. In Mo- and Ni-doped TiO_2, the dopant ions enter the anatase lattice and influence the level of oxygen vacancies, thereby promoting the transformation of anatase to rutile phase below 500 °C. Cr inthe TiO_2 matrix also increases the anatase–rutile transition but the necessary temperature for transition is above 600 °C, and therefore the rutile phase was not expected in Cr-doped TiO_2, as the catalysts were calcined at only 500 °C [29, 36, 37].

Diffuse reflectance spectra of synthesized catalysts are shown in Fig. 2. The observed spectra display the typical absorption behavior of a wide band gap semiconductor. TiO_2 and Cr/TiO_2 exhibited the strongest absorption at lower wavelengths corresponding to band gap energies of 3.27 and 3.11 eV, respectively, followed by Mo/TiO_2 (2.73 eV) and Ni/TiO_2 (2.71 eV). The metal ions used in this study had valence states differing from that of Ti (+4), resulting into an impurity level in the band gap and creating vacancies in the oxygen sites, which in turn may have resulted in the absorption of light in the visible spectrum [22, 24, 27, 31, 38, 39].

BET surface area, pore volume and average pore diameter of the synthesized catalysts are shown in Table 1. The highest specific surface areas, of 71.4 and 62.1 m^2/g, were obtained with sol–gel-synthesized TiO_2 and Mo/TiO_2 photocatalysts, respectively, compared to 23.0 m^2/g of Cr-doped TiO_2, and 35.2 m^2/g of Ni/TiO_2. The average pore volumes for TiO_2, Cr/TiO_2, Mo/TiO_2 and Ni/TiO_2 were found to be 0.24, 0.041, 0.11 and 0.053 cm^3/g, respectively. The average pore diameter for TiO_2 was 136 Å, for Cr/TiO_2 and Mo/TiO_2 it was 72 Å, whereas, for Ni/TiO_2, it was found to be 60 Å.

Surface morphology of the synthesized catalysts was investigated using FE-SEM and elemental composition was obtained using EDX, as shown in Fig. 3. The particles can be observed as spherical shaped and mostly present in the form of aggregates (lumps). EDX spectra indicated 0.29, 0.92 and 0.81% doping of Cr, Mo
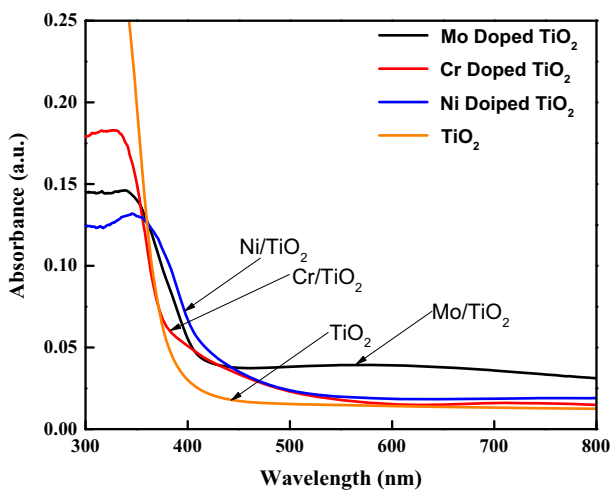

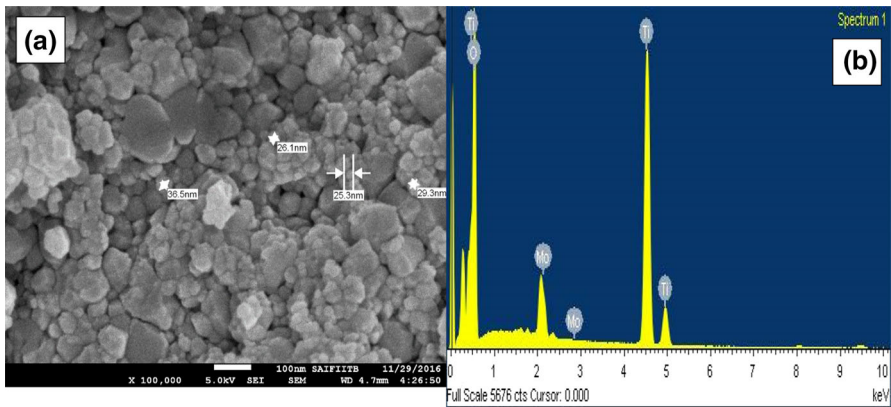**Fig. 2** Diffuse reflectance spectra of TiO_2, Cr/TiO_2, Mo/TiO_2 and Ni/TiO_2 catalysts

Fig. 3 **a** FE-SEM image and **b** EDX spectra of MO/TiO$_2$ catalyst

and Ni, respectively, in the catalysts. Further, the Mo/TiO$_2$ was also characterized by TEM and the results are presented in Fig. 4. The crystallite size of Mo/TiO$_2$ obtained from the TEM image (Fig. 4a) was found to be 30 nm, which was in agreement with the crystallite size calculated from XRD. Figure 4b shows a dark field image of diffraction rings. Analysis confirmed that the rings corresponded to the (101), (105), (116), (211), (200) and (204) crystalline planes of the anatase as well as the (110) plane of the rutile phase.

XPS measurements were carried out to investigate the oxidation states of the elements in the doped catalysts. XPS survey spectra of Mo/TiO$_2$, Cr/TiO$_2$ and Ni/TiO$_2$ are shown in Fig. 5a–c, respectively. Carbon was used as the reference material and its characteristic peak appeared around 285 eV in Fig. 5a–c [40]. The peaks observed at 457.2 eV and 463 eV are attributed to Ti 2p$_{3/2}$ and Ti 2p$_{1/2}$ electrons, respectively, (Fig. 5a–c) which confirmed the presence of Ti^{4+} species in the TiO$_2$ lattice. Double peaks at 231 eV and 234.5 eV in Fig. 5a are due to Mo 3d5/2 and Mo 3d3/2 states in Mo^{4+}, and double peaks at 528.5 and 530.5 due to O
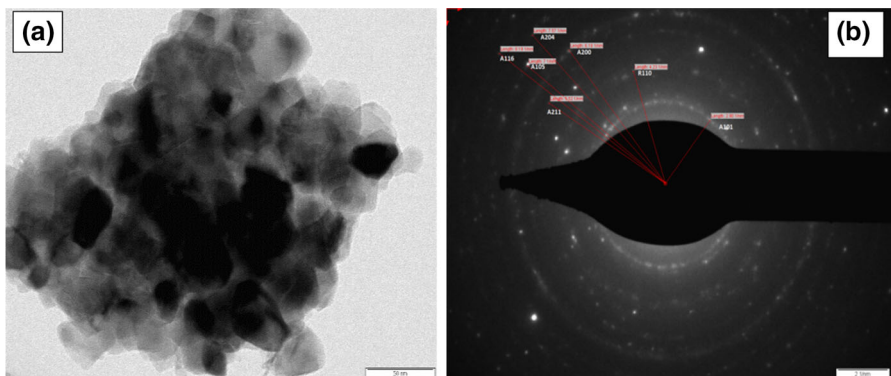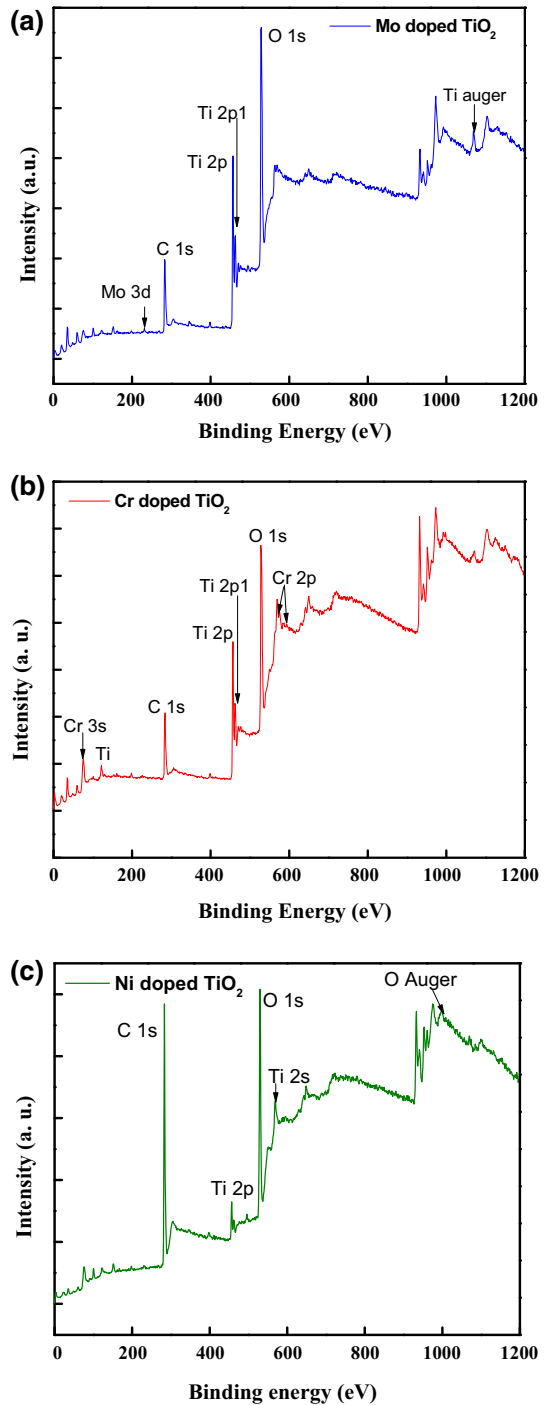

Fig. 4 **a** TEM image and **b** electron diffraction pattern of Mo/TiO$_2$ catalyst

Fig. 5 XPS spectra of synthesized catalysts: **a** Mo-doped TiO_2, **b** Cr-doped TiO_2, **c** Ni-doped TiO_2

1 s in TiO_2 and MoO_2 were observed [41]. Each Mo atom in MoO_2 is coordinated to six oxygen atoms similar to that in rutile TiO_2. Figure 5b gives the XPS spectra of Cr-doped TiO_2. Peaks located at the binding energy of 75 eV (Cr 3 s), 575.8 eV (Cr $2p_{3/2}$) and 586 eV (Cr $2p_{1/2}$) indicating the presence of Cr^{3+} in the sample can be observed. Additionally, peaks due to O 1 s in TiO_2 and Cr_2O_3 were observed at 528.4 eV and 530.4 eV, respectively [42, 43]. For reasons which are unclear, no peaks corresponding to Ni were visible in the XPS spectra of Ni-doped TiO_2. The binding energies of Mo 3d and Cr 2p agreed with those of MoO_2 and Cr_2O_3, respectively, which, coupled with a lack of peaks for MoO_2 and Cr_2O_3 in the XRD spectra, provide evidence of the substitution of Mo and Cr in the TiO_2 matrix as Mo^{4+} and Cr^{3+}, respectively.

Photocatalytic degradation studies

The activity of synthesized catalysts was investigated from the photocatalytic degradation studies on MB dye as a target compound. In heterogeneous catalysis, mass transfer limitations may hinder the study of intrinsic catalytic activity. The effect of agitation on the photocatalytic degradation of MB was studied to ascertain external mass transfer limitations. It was observed that any stirring speed between 300 and 700 rpm resulted in no significant change in the reaction; therefore, further experiments were performed at 500 rpm. Intra-particle mass transfer limitations may also play a role in affecting the discovery of intrinsic kinetics, and hence the Weisz–Prater criterion was applied to pseudo-first-order reaction kinetics and the value of N_{W-P} was found to be 6.15×10^{-6} which is less than 3β (= 4.8).

For initial studies, a loading of 1 g/L was selected based on reported photocatalytic degradation studies. The effect of bare and doped (with Cr, Mo and Ni) TiO_2 catalysts on the photocatalytic degradation of a 10-ppm MB solution in the presence of UV light as well as sunlight was studied, as shown in Fig. 6a, b, respectively. The results obtained in the above experiments were also compared with control experiments, namely, dark (no light but in the presence of a catalyst) and photolysis (no catalyst but in the presence of light). We found no significant MB degradation in UV or visible photolysis experiments [25, 38, 44].

Among the doped catalysts, Mo/TiO_2 showed the highest photocatalytic activity, and % dye degradation was observed to be 98 and 95% in the presence of UV and visible light, respectively. % dye degradation with TiO_2, Cr/TiO_2 and Ni/TiO_2 catalysts was observed as 50, 25 and 24%, respectively, in UV light, whereas, with visible light, the % dye degradation with TiO_2, Cr/TiO_2 and Ni/TiO_2 catalysts was observed to be 65, 52 and 48%, respectively. Anatase TiO_2 is a very active photocatalyst with fast electron–hole pair generation and recombination. Rutile phase TiO_2 is denser and shows slower electron–hole generation and recombination. In mixed phase TiO_2, the electron–hole recombination are slowed, further improving carrier lifetime [45–48]. The longer the carrier lifetime, the higher is the probability that the carriers will participate in surface reactions. Consequently, a mixed phase catalyst is more active. Mo-doped TiO_2 and Ni-doped TiO_2 show mixed anatase and rutile phases, whereas TiO_2 and Cr-doped TiO_2 show only the anatase phase. The activity of Ni-doped TiO_2 and Mo-doped TiO_2, therefore, is
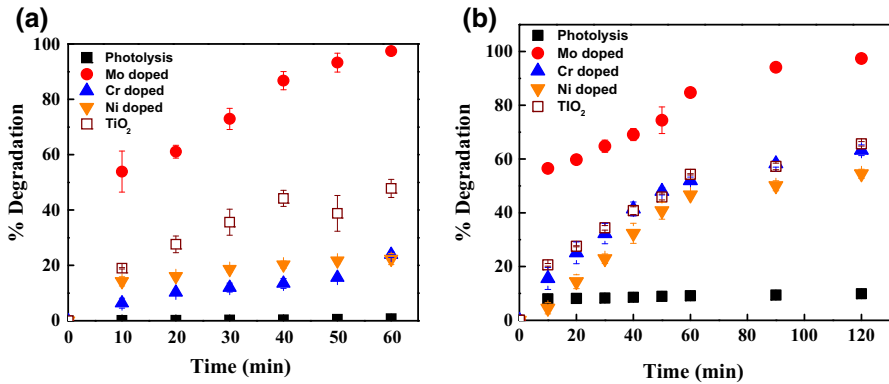
Fig. 6 Effect of metal-doped TiO_2 on the photocatalytic degradation of MB dye. **a** UV irradiation; conditions: catalyst loading: 1 g/L, dye concentration: 10 ppm; photolysis (*filled square*), Mo-doped TiO_2 (*filled circle*), Cr-doped TiO_2 (*filled upward-pointing triangle*), Ni-doped TiO_2 (*filled downward-pointing triangle*), TiO_2 (*open square*); **b** solar irradiation: catalyst loading: 1 g/L, dye concentration: 10 ppm; photolysis (*filled square*), Mo-doped TiO_2 (*filled circle*), Cr-doped TiO_2 (*filled upward-pointing triangle*), Ni-doped TiO_2 (*filled downward pointing triangle*), and TiO_2 (*open square*)

expected to be higher than TiO_2 and Cr-doped TiO_2. The surface area of Cr-doped TiO_2 and Ni-doped TiO_2 was much lower than that of TiO_2 and Mo-doped TiO_2. The higher the surface area, the higher the number of active surface sites are available to convert absorbed water molecules to active hydroxyl and superoxide radicals by action of the photo-generated holes, which in turn brings about the degradation of organic pollutants [49, 50]. Thus, with a combination of the effect of the presence of polymorphs and differing surface areas, the order of activity of Mo-doped $TiO_2 >$ $TiO_2 >$ Ni-doped $TiO_2 >$ Cr-doped TiO_2 was observed.

Thus, detailed experiments to study the effect of catalyst loading, initial dye concentration and pH were carried out with Mo/TiO_2. The effect of catalyst loading was varied in the range of 0.3–2 g/L. Figure 7 show the results obtained in the above experiments in the presence of UV and visible light, respectively. At a low catalyst loading of 0.1 and 0.3 g/L, % degradation in the presence of UV light was observed as 69 and 76%, respectively, whereas, in the presence of visible light, the % degradation was observed as 76 and 82%, respectively. Increasing the catalyst loading to 0.5, 0.75, 1 and 1.5 g/L increased the % degradation to 82, 83, 89, and 97%, respectively, in the presence of UV light, whereas, the % degradation in the presence of visible light increased to 86, 89, 92, and 97%, respectively. The catalyst loading above 1.5 g/L resulted in decreased degradation, irrespective of the light source. The % degradation with 2 g/L in the presence of UV and visible light was observed as 93 and 92%, respectively. Figures 7b and 8b show the variation in the % degradation with respect to catalyst concentration at the end of 60 min and 120 min in the presence of UV and visible light, respectively. Thus, 1.5 g/L was observed as the optimum catalyst loading in the presence of either of the light sources.

Previous studies have reported an optimum catalyst loading in the range of 1.0–1.5 g/L [51–54]. A comparison of catalytic activity of doped TiO_2 catalysts reported in open diamondliterature is presented in Table 2. During photocatalysis,
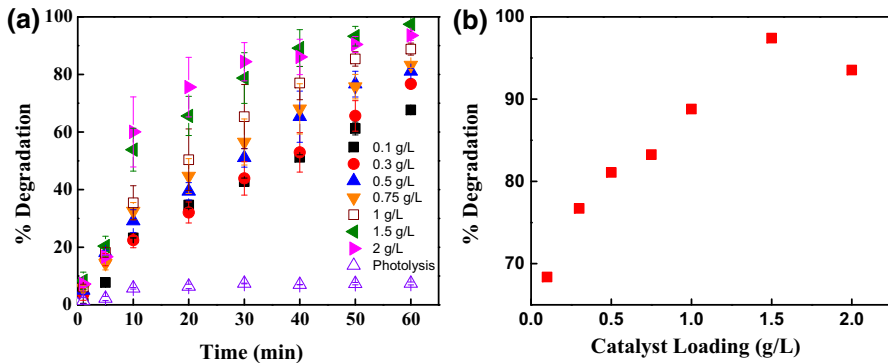
Fig. 7 **a** Effect of Mo/TiO$_2$ loading on photocatalytic degradation of MB dye under UV irradiation; 0.1 g/L (*filled square*), 0.3 g/L (*filled circle*), 0.5 g/L (*filled upward-pointing triangle*), 0.75 g/L (*filled downward-pointing triangle*), 1 g/L (*open square*), 1.5 g/L (*filled left-pointing triangle*), 2 g/L (*open diamond*), photolysis (*open upward-pointing triangle*); **b** % degradation of MB against catalyst loading in UV light after 60 min
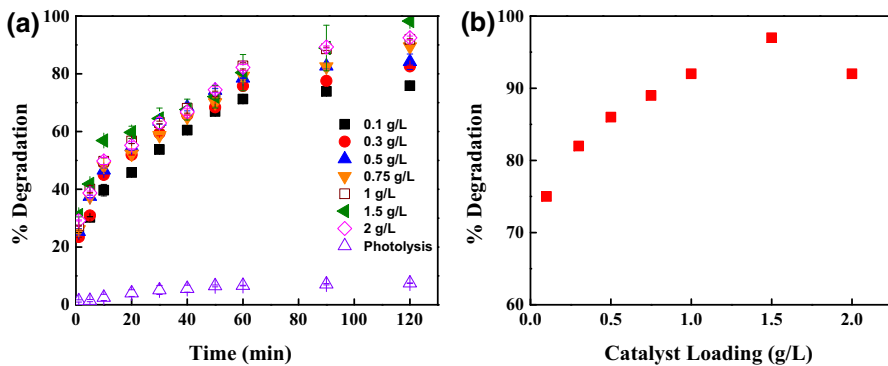

Fig. 8 **a** Effect of Mo/TiO$_2$ loading on photocatalytic degradation of MB dye under solar irradiation; 0.1 g/L (*filled square*), 0.3 g/L (*filled circle*), 0.5 g/L (*filled upward-pointing triangle*), 0.75 g/L (*filled downward-pointing triangle*), 1 g/L (*open square*), 1.5 g/L (*filled sideways-pointing triangle*), 2 g/L (*open diamond*), photolysis (*open triangle*); **b** % degradation of MB against catalyst loading in solar light after 120 min

an increase in catalyst loading increases the amount of reactive oxygen species and thereby increases the degradation. However, the increased reaction rate is usually limited by the obstruction in the transmission of light due to open diamondpresence of excess amounts of catalyst (also known as the shadowing or screening effect), which reduces the specific activity of the catalyst [51, 55–57].

Figure 9a, b shows the effect of dye concentration on the MB degradation under UV and solar irradiation, respectively. The experiments were carried out at a catalyst loading of 1.5 g/L and the initial dye concentration was varied in the range of 10–50 ppm. It was observed that the % degradation decreased with increasing

Table 2 Photocatalytic studies using Mo-doped TiO_2 catalyst for degradation of MB dye

S. no.	Catalyst	Catalyst loading (g/L)	Cut-off wavelength (nm)	Band gap (eV)	Source of light	Capacity (W)	Irradiation time (min)	Degradation (%)	Reference
1	Mo/TiO$_2$	1.5	450	2.73	Mercury vapor lamp	125	60	98	Our work
2	Mo/TiO$_2$	1.5	450	2.73	Solar	–	60	88	Our work
3	Ni/TiO$_2$	1.5	450	2.71	Mercury vapor lamp	125	60	21	Our work
4	Ni/TiO$_2$	1.5	450	2.71	Solar	–	120	58	Our work
5	Cr/TiO$_2$	1.5	420	3.02	Mercury vapor lamp	125	60	24	Our work
6	Cr/TiO$_2$	1.5	420	3.02	Solar	–	120	65	Our work
7	Cr/TiO$_2$	0.5	415	3.13	Mercury vapor lamp	300	180	43	Zhang et al. [20]
8	Cr/TiO$_2$	0.1	–	–	Blue light tubes	80	2160	99	Wei et al. 28
9	Mo/TiO$_2$	2	421	2.94	Xenon lamp	500	300	78	Huang et al. 17
10	Mo/TiO$_2$	2	454	2.73	Solar	–	300	94	Huang et al. 17
11	Mo/TiO$_2$	5	450	2.65	Mercury vapor lamp	250	60	96	Majeed et al. 38
12	Mo/TiO$_2$	0.39	450	2.6	Xenon lamp	500	180	40	Tan et al. 31
13	Mo/TiO$_2$	1.8	350	3.2	Mercury vapor lamp	50	120	65	Luo et al. 24
14	Mo/TiO$_2$	0.125	444	2.8	Mercury vapor lamp	300	60	88	Khan and Berk 25
15	Mo/TiO$_2$	1	–	–	Mercury vapor lamp	125	80	40	Yang et al. 26
16	Mo/TiO$_2$	2	410	3.05	Mercury vapor lamp	250	150	75	Wang et al. 27
17	Mo/TiO$_2$	2	410	3.05	Xenon lamp	300	150	73	Wang et al. 27

Table 2 continued

| S. no.	Catalyst	Catalyst loading (g/L)	Cut-off wavelength (nm)	Band gap (eV)	Source of light	Capacity (W)	Irradiation time (min)	Degradation (%)	Reference
18	Mo/TiO$_2$	0.06 + (NH$_4$)$_2$S$_2$O$_8$	480	2.5	Mercury vapor lamp	125	120	93	Gomathi Devi et al. 22
19	Mo/TiO$_2$	1	254	2.95	Mercury vapor lamp	450	120	95	Avilés-García et al. [62]
20	Ni/TiO$_2$	0.1	410	3.08	Xenon lamp	1000	240	96	Ibram et al. [63]
21	Ni/TiO$_2$	1.5	–	–	Mercury vapor lamp	500	120	90	Yu et al. 21

(a)

(b)
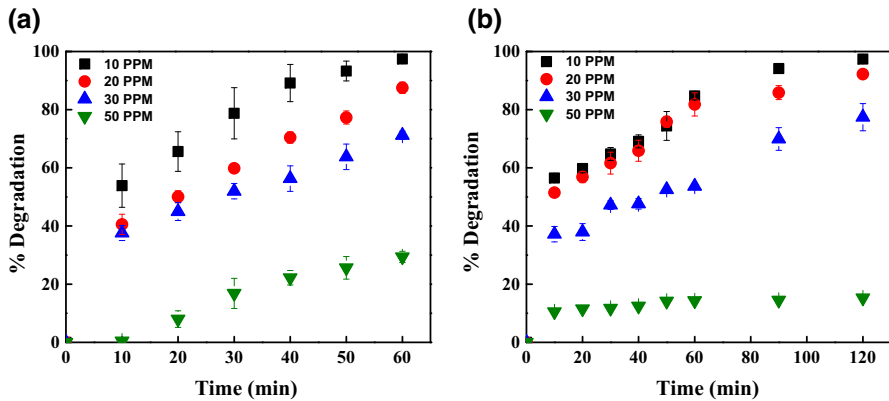
Fig. 9 **a** Effect of initial dye concentration on photocatalytic degradation of MB dye using UV irradiation; 10 ppm (*filled square*), 20 ppm (*filled circle*), 30 ppm (*filled upward-pointing triangle*), 50 ppm (*filled downward-pointing triangle*); **b** solar irradiation; 10 ppm (*filled square*), 20 ppm (*filled circle*), 30 ppm (*filled upward-pointing triangle*), 50 ppm (*filled downward-pointing triangle*)). Catalyst loading 1.5 g/L

initial dye concentration, irrespective of the light source. In the presence of UV light, the % degradation with an initial dye concentration of 10, 20, 30 ppm and 50 was 97, 80, 71, and 29%, respectively. On the other hand, in the presence of visible light, the % degradation with an initial dye concentration of 10, 20, 30 and 50 ppm was 97, 93, 80, and 15%, respectively. With an increase in initial dye concentration, the amount of dye adsorbed on the active sites increases, which are likely to block the active sites of catalyst and result in reduced rates of degradation. The photocatalytic activity of the catalysts is inversely proportional to the concentration of MB in solution [16, 31, 55, 58, 59].

Figures 10 and 11 show the activity of Mo-doped TiO_2 under UV and solar irradiation, respectively, for the degradation of MB at various pH (3–11). Increasing the solution pH from 3 to 5 and 7 increased the degradation from 32 to 38%, and 97%, respectively, under UV. In the presence of visible light, the % degradation increasing the solution pH from 3 to 5 and 7 increased the degradation from 28 to 62, and 98%, respectively. However, further increase in the solution pH to 9 and 11 resulted in no change in the degradation and the results were similar to that obtained at solution pH of 7.

$$TiOH + H^+ \rightleftharpoons TiOH_2^+ \qquad (2)$$

$$TiOH + OH^- \rightleftharpoons TiO^- + H_2O \qquad (3)$$
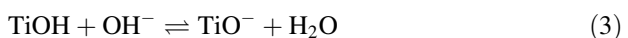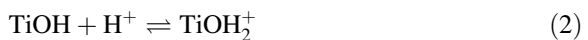
TiO_2 is hydrated to give Ti–OH groups on the surface [51]. In acidic pH, TiO_2 takes up H^+ ions and acquires a positive charge, whereas, in basic pH, TiO_2 loses protons to OH^- ions and acquires a negative charge. MB is a cationic dye and, therefore, will preferentially adsorb on negatively charged TiO_2. However, the dye becomes positively charged in acidic solutions while remaining as a neutral
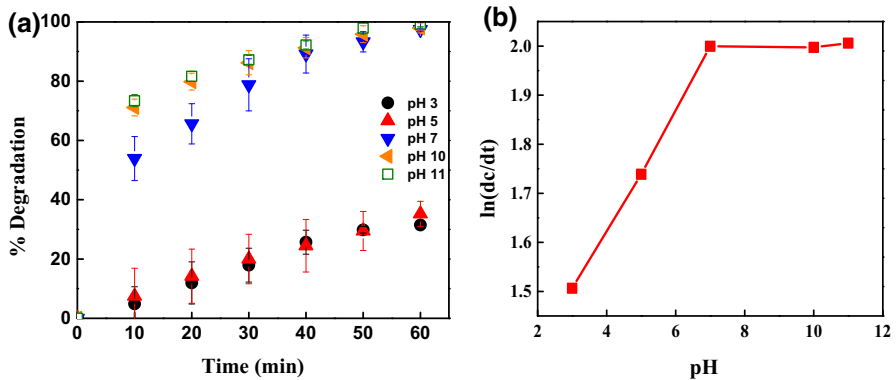
Fig. 10 a Effect of pH on photocatalytic degradation of MB dye using UV irradiation; pH 3 (*filled circle*), pH 5 (*filled upward–pointing triangle*), pH 7 (*filled downward-pointing triangle*), pH 10 (*filled left-pointing triangle*), pH 11 (*open square*); **b** the initial rate of the reaction [ln(dc/dt)] against pH of the solution; **b** initial rate of degradation plotted against the pH on semi-log scale. Conditions: catalyst = Mo-doped TiO$_2$; catalyst loading = 1.5 g/L; dye concentration: 10 ppm; light source: UV light
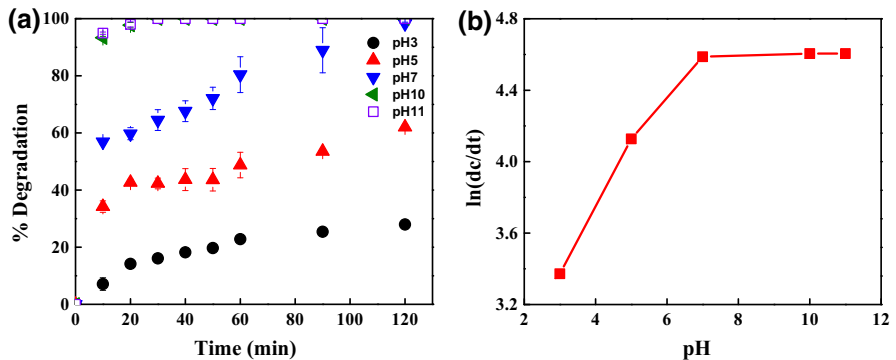

Fig. 11 a Effect of pH on photocatalytic degradation of MB dye using solar irradiation; pH 3 (*filled circle*), pH 5 (*filled upward-pointing triangle*), pH 7 (*filled downward-pointing triangle*), pH 10 (*filled left-pointing triangle*), pH 11 (*open square*); **b** the initial rate of the reaction [ln(dc/dt)] against pH of the solution; **b** Initial rate of degradation plotted against the pH on semi-log scale. Conditions: catalyst = Mo-doped TiO$_2$; catalyst loading = 1.5 g/L; dye concentration: 10 ppm; light source: solar light

molecule in basic solutions. In acidic solutions, due to electrostatic repulsion, the rate of adsorption of MB on TiO$_2$ decreases, lowering the rate of degradation [61].

Our studies revealed extremely high activity of the Mo-doped catalyst compared to earlier reports. We obtained > 98 and 88% degradation of 10 ppm MB in 60 and 120 min of UV and solar light, respectively. Other studies have reported as much as twice the amount of time for a similar degradation, using a much higher-powered

UV source for irradiation. Moreover, we have not used any other co-oxidant such as hydrogen peroxide or ammonium persulfate for degradation. Further, there are no reports that compare the catalytic activity of Mo-doped TiO_2 for both UV and solar light catalysis. The amount of dopant we have used is also less; other reports have used higher amounts of Mo in TiO_2 to achieve photocatalysis [17, 20, 21, 25, 31, 35, 40, 45]. Therefore, the catalysts we report exhibit much higher activity. Degradation products of methylene were also identified using HR-LCMS and a plausible mechanism is presented.

Kinetic analysis

The photocatalytic degradation of dye is reported to follow a pseudo-first order kinetics model [18, 26, 48, 50]. Therefore, at optimum reaction conditions, the experimental data for photocatalytic degradation of the MB under UV and sunlight were validated using a pseudo-first order kinetics model and the results are shown in Fig. 12a, b. The pseudo-first-order rate constants, k_{app} for the photocatalytic degradation of dye using Mo/TiO_2 with UV and solar light were obtained from the slope of the linear fit and were found to be 0.056 and 0.0301 min^{-1}, respectively. It can be seen that a good correlation of pseudo-first-order reaction kinetics was found.

Mechanism of degradation

The reaction intermediates were analysed by HR-LCMS and the chromatogram of the reaction mixture is shown in Fig. S2. A plausible degradation mechanism is proposed in Fig. 13 based on the LCMS data. The degradation proceeds via the loss of methyl groups of tertiary amines (II) to give the primary amino-substituted intermediate (IV). An alternative pathway proceeds by the attack of hydroxyl radicals on the heteroatoms in the MB ring resulting in the fracture of C-N and attack on the C–S^+=C cation (V) and other intermediates (VI, XI, XII) before splitting up into two (VI and VII), further giving catechol (VIII) and phenol (IX) [60].
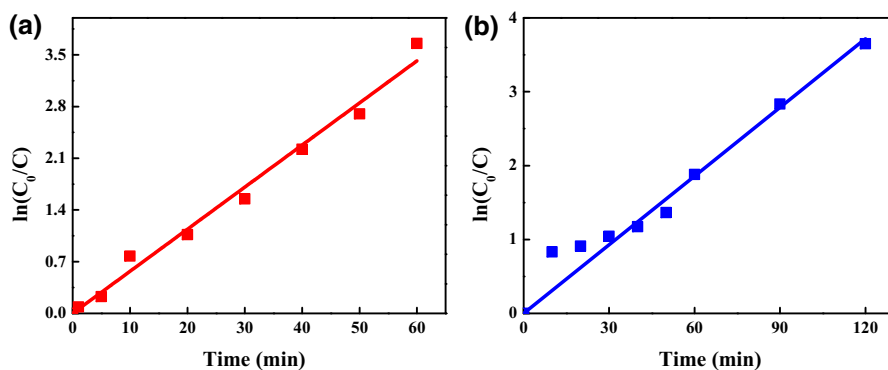

Fig. 12 First-order kinetics validation of the experimental data: **a** UV light, **b** solar light (optimum conditions catalyst loading = 1.5 g/L; dye concentration: 10 ppm, pH = 7)
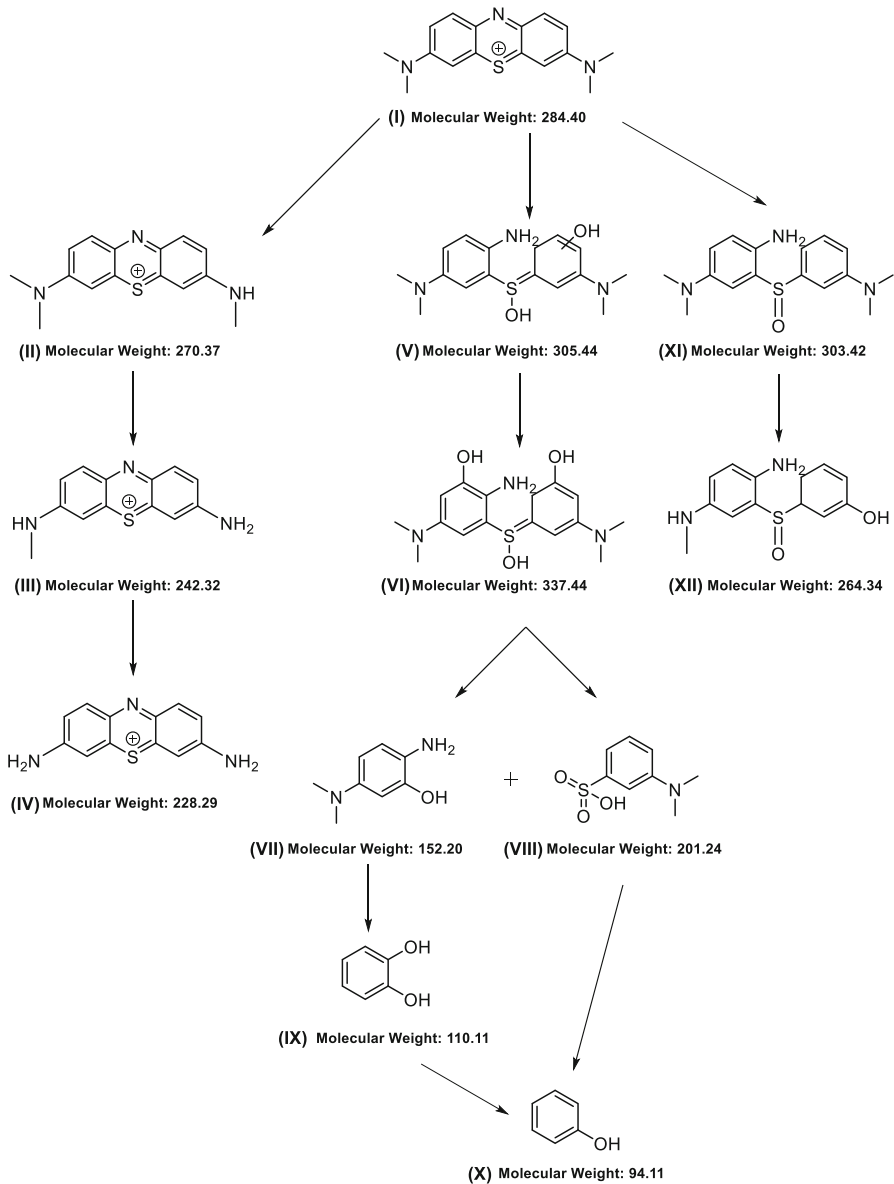
Fig. 13 Proposed degradation pathway for photocatalytic degradation of MB dye

Conclusion

We have synthesized molybdenum-, chromium- and nickel-doped titania using a facile sol–gel route. Doping decreased the band gap of TiO_2 from 3.2 to 2.83 eV for Mo-doped TiO_2. Consequently, Mo-doped TiO_2 is also active in the visible region. Among the catalysts synthesized, Mo-doped TiO_2 was the most active, and 98%

degradation of MB was obtained for Mo-doped TiO_2 in 60 min under UV light irradiation and in 120 min under solar light. The catalyst is active in solar light at a catalyst loading as low as 0.75 g/L. Optimum catalyst loading was found to be 1.5 g/L for both UV and solar irradiation. The rRate of degradation was found to be higher at higher pH. Synthesized Mo-doped TiO_2 was compared with other reports and was found to be much more active at a lower or similar concentration under much weaker light irradiation. In conclusion, we have developed an active catalyst that can be used for the degradation of dye effluents under solar light photocatalysis.

References

1. N. Chekir, O. Benhabiles, D. Tassalit, N.A. Laoufi, F. Bentahar, Desalin. Water Treat. **57**, 6141 (2016)
2. M. Muruganandham, M. Swaminathan, Dyes Pigment **72**, 137 (2007)
3. K. Bubacz, J. Choina, D. Dolat, A.W. Morawski, Pol. J. Environ. Stud **19**, 685 (2010)
4. S. Sadri Moghaddam, M.R. Alavi Moghaddam, M. Arami, J Hazard Mater **175**, 651 (2010)
5. L.-G. Wang, G.-B. Yan, Desalination **274**, 81 (2011)
6. L. Zheng, X. Wang, X. Wang, J. Clean Prod. **108**, 525 (2015)
7. J.H.B. Rocha, M.M.S. Gomes, E.V. dos Santos, E.C.M. de Moura, D.R. da Silva, M.A. Quiroz, C.A. Martínez-Huitle, Electrochim. Acta **140**, 419 (2014)
8. H. Ali, Water Air Soil Pollut. **213**, 251 (2010)
9. G.G. Bessegato, J.C. Cardoso, B.F. da Silva, M.V.B. Zanoni, Appl. Catal. B Environ. **180**, 161 (2016)
10. P. Liang, M. Rivallin, S. Cerneaux, S. Lacour, E. Petit, M. Cretin, J. Membr. Sci. **510**, 182 (2016)
11. B. Brunekreef, S.T. Holgate, The Lancet **360**, 1233 (2002)
12. M. Anpo, M. Takeuchi, J. Catal. **216**, 505 (2003)
13. S. Malato, P. Fernández-Ibáñez, M.I. Maldonado, J. Blanco, W. Gernjak, Catal. Today **147**, 1 (2009)
14. M.I. Litter, Appl. Catal. B Environ. **23**, 89 (1999)
15. M. Pelaez, N.T. Nolan, S.C. Pillai, M.K. Seery, P. Falaras, A.G. Kontos, P.S.M. Dunlop, J.W.J. Hamilton, J.A. Byrne, K. O'Shea, M.H. Entezari, D.D. Dionysiou, Appl. Catal. B Environ. **125**, 331 (2012)
16. Ö. Kerkez-Kuyumcu, E. Kibar, K. Dayıoğlu, F. Gedik, A.N. Akın, Ş. Özkara-Aydınoğlu, J. Photochem. Photobiol. Chem. **311**, 176 (2015)
17. J. Huang, X. Guo, B. Wang, L. Li, M. Zhao, L. Dong, X. Liu, Y. Huang, J. Spectrosc. **2015**, e681850 (2015)
18. S.N.R. Inturi, T. Boningari, M. Suidan, P.G. Smirniotis, Appl. Catal. B Environ. **144**, 333 (2014)
19. G. M. Madhu, A. Raj, M. A. Lourdu, K. V. K. Pai, and S. Rao, IJCT Vol142 March 2007 (2007)
20. S. Zhang, Y. Chen, Y. Yu, H. Wu, S. Wang, B. Zhu, W. Huang, S. Wu, J. Nanoparticle Res. **10**, 871 (2008)
21. K. Yu, M. Song, X. Gao, C. Hou, J. Liang, Synth. React. Inorg. Met.-Org. Nano-Met. Chem. **45**, 1576 (2015)
22. L. Gomathi Devi, B. Narasimha Murthy, S. Girish Kumar, Chemosphere **76**, 1163 (2009)
23. W. Choi, A. Termin, M.R. Hoffmann, J. Phys. Chem. **98**, 13669 (1994)
24. S.-Y. Luo, B.-X. Yan, J. Shen, Thin Solid Films **522**, 361 (2012)
25. H. Khan, D. Berk, J. Photochem. Photobiol. Chem. **294**, 96 (2014)
26. Y. Yang, X. Li, J. Chen, L. Wang, J. Photochem. Photobiol. Chem. **163**, 517 (2004)
27. S. Wang, L.N. Bai, H.M. Sun, Q. Jiang, J.S. Lian, Powder Technol. **244**, 9 (2013)
28. Y.-L. Wei, K.-W. Chen, H.P. Wang, J. Nanosci. Nanotechnol. **10**, 5456 (2010)
29. M. Prekajski, A. Zarubica, B. Babić, B. Jokić, J. Pantić, J. Luković, B. Matović, Ceram. Int. **42**, 1862 (2016)
30. G.G. Nakhate, V.S. Nikam, K.G. Kanade, S. Arbuj, B.B. Kale, J.O. Baeg, Mater. Chem. Phys. **124**, 976 (2010)
31. K. Tan, H. Zhang, C. Xie, H. Zheng, Y. Gu, W.F. Zhang, Catal. Commun. **11**, 331 (2010)

32. R. Vijayalaxmi, V. Rajendran, Arch. Appl. Sci. Res. **4**, 1183 (2012)
33. S. Tambat, S. Umale, S. Sontakke, Mater. Res. Bull. **76**, 466 (2016)
34. S. Li and P. Jena, Phys. Rev. B **79**, (2009)
35. D.A.H. Hanaor, C.C. Sorrell, J. Mater. Sci. **46**, 855 (2011)
36. L. Yuan, X. Weng, M. Zhou, Q. Zhang, L. Deng, Nanoscale Res. Lett. **12**, 597 (2017)
37. R.S. Dubey, S. Singh, Results Phys. **7**, 1283 (2017)
38. J. Majeed, C. Nayak, S.N. Jha, K. Bhattacharyya, D. Bhattacharyya, A.K. Tripathi, RSC Adv. **5**, 90932 (2015)
39. S. Wang, X. Hai, X. Ding, K. Chang, Y. Xiang, X. Meng, Z. Yang, H. Chen, and J. Ye, Adv. Mater. **29**, 1701774 (2017)
40. H. Zhu, J. Tao, X. Dong, J. Phys. Chem. C **114**, 2873 (2010)
41. B. Brox, I. Olefjord, Surf. Interface Anal. **13**, 3 (1988)
42. E. Agostinelli, C. Battistoni, D. Fiorani, G. Mattogno, M. Nogues, J. Phys. Chem. Solids **50**, 269 (1989)
43. Y.-H. Peng, G.-F. Huang, W.-Q. Huang, Adv. Powder Technol. **23**, 8 (2012)
44. E. Alzahrani, Am. J. Anal. Chem. **8**, 95 (2017)
45. T. van der Meulen, A. Mattson, L. Österlund, J. Catal. **251**, 131 (2007)
46. W.R. Siah, H.O. Lintang, M. Shamsuddin, L. Yuliati, I.O.P. Conf, Ser. Mater. Sci. Eng. **107**, 012005 (2016)
47. A. Kafizas, C.J. Carmalt, I.P. Parkin, Chem.-Eur. J. **18**, 13048 (2012)
48. M. Boehme, W. Ensinger, Nano-Micro Lett. **3**, 236 (2011)
49. H. Hassena, Mod. Chem. Appl. **4**, (2016)
50. J. Wen, X. Li, W. Liu, Y. Fang, J. Xie, Y. Xu, Chin. J. Catal. **36**, 2049 (2015)
51. M. Ahsan Habib, I.M.I. Ismail, A.J. Mahmood, M. Rafique Ullah, J. Saudi, Chem Soc **16**, 423 (2012)
52. P. Nuengmatcha, S. Chanthai, R. Mahachai, W.-C. Oh, Dyes Pigments **134**, 487 (2016)
53. S.K. Kansal, N. Kaur, S. Singh, Nanoscale Res. Lett. **4**, 709 (2009)
54. A. Daya Mani, B. Rama Raju, N. Xanthopoulos, P. Ghosal, B. Sreedhar, C. Subrahmanyam, Chem. Eng. J. **228**, 545 (2013)
55. R.S. Dariani, A. Esmaeili, A. Mortezaali, S. Dehghanpour, Opt. Int. J. Light Electron Opt. **127**, 7143 (2016)
56. J. Sun, X. Wang, J. Sun, R. Sun, S. Sun, L. Qiao, J. Mol. Catal. Chem. **260**, 241 (2006)
57. U.G. Akpan, B.H. Hameed, J. Hazard. Mater. **170**, 520 (2009)
58. K.M. Reza, A.S.W. Kurny, F. Gulshan, Appl. Water Sci. 1 (2015)
59. R.M. Mohamed, I.A. Mkhalid, E.S. Baeissa, M.A. Al-Rayyani, J. Nanotechnol. **2012**, e329082 (2012)
60. A. Houas, H. Lachheb, M. Ksibi, E. Elaloui, C. Guillard, J.-M. Herrmann, Appl. Catal. B Environ. **31**, 145 (2001)
61. G.S. Singhal, E. Rabinowitch, J. Phys. Chem. **71**, 3347 (1967)
62. O. Avilés-García, J. Espino-Valencia, R. Romero, J.L. Rico-Cerda, M. Arroyo-Albiter, R. Natividad, Fuel **198**, 31 (2017)
63. G. Ibram, A.K. Gupta, P.P. Kumar, P.S.C. Sekhar, K. Radha, G. Padmananbham, G. Sundararajan, Sci. World J. **2012**, 1 (2012)